Construction and Building Materials 185 (2018) 414–422

Contents lists available at ScienceDirect

Construction and Building Materials

journal homepage: www.elsevier.com/locate/conbuildmat

Evaluation of the performance of sensor-enabled geobelts after cyclic loading

Xin-zhuang Cui *, She-qiang Cui, Tu Lu, Lei Zhang, Yi-lin Wang, Jun Li

School of Civil Engineering, Shandong University, Jinan 250061, PR China

HIGHLIGHTS

- A new smart geosynthetic named sensor-enabled geobelt (SEGB) was developed.
- The effects of prestrains and cyclic loads on SEGB were investigated.
- Mechanical properties of SEGB after cyclic loading were evaluated.
- A preliminary model was proposed to evaluate tensoresistivity of SEGB.

ARTICLE INFO

Article history:
Received 17 January 2018
Received in revised form 21 June 2018
Accepted 9 July 2018

Keywords:
Sensor-enabled geobelts
Tensoresistivity
Cyclic loading
Prestrain

ABSTRACT

Geosynthetics are an effective method to increase the seismic level of reinforcement soil structures. In this paper, sensor-enabled geobelts (SEGB) that performed self-measurement and reinforcement functions were developed on the strain-sensitive electrical conductivity (tensoresistivity) of the high-density polyethylene (HDPE) filled with super conductive carbon black (CB). To study the influence of seismic loads on SEGB, a series of cyclic loading tests were performed. Before cyclic loading, different prestrains were applied to simulate the deformation of SEGB in soil before earthquake. The results show that the tensile strength and elongation at break of SEGB after cyclic loading decrease with the number of loading cycles and strain amplitude of cyclic load, though the prestrains have a limited influence on the reduction of mechanical properties of SEGB. For the tensoresistivity response of SEGB after cyclic loading, the electrical conductivity of SEGB becomes more sensitive to strain by increasing number of loading cycles, amplitude of cyclic load and prestrains. Based on the test results, a preliminary model was proposed to evaluate the tensoresistivity performance of SEGB after cyclic loading.

1. Introduction

Geosynthetic engineering has experienced tremendous growth over the past few decades. Geosynthetic reinforcements are widely used to improve the stability of many kinds of soil structures. Examples include the stabilization of highway slopes and embankments [1,2], reinforcement of foundations [3–5], and reinforcement of paved roads to mitigate cracking and rutting [6]. As geosynthetic reinforcements are used in a wide range of soil structures and these structures are subjected to various loading conditions including static and dynamic loads, more and more attention has been paid to evaluating the performance of geosynthetic-reinforced soil structures under static and dynamic loads by numerical calculations, laboratory and field tests, etc. For example, experimental studies involving field and laboratory static loading tests on geosynthetic-reinforced soil structures have been conducted [7–11]. Besides the response under static loads, there also have been many studies performed on the behaviors of geosynthetic-reinforced soil structures under dynamic loads. For instance, in order to investigate the dynamic behaviors of geosynthetic-reinforced soil structures, model tests under seismic loading had been done by some researchers [12–18]. In summary, these studies on geosynthetic-reinforced soil structures are helpful to obtain comprehensive knowledge on the behaviors of geosynthetics under static and dynamic loads, which also contribute more to the development of geosynthetics. It is also noted that these studies mostly pertain to the area wherein the soil is reinforced with geogrids, geocells, geotextiles. However, geobelt, made of polymeric materials, is one of the reinforcement materials and has also been widely used as reinforcement in embankment and

* Corresponding author.
E-mail addresses: cuixz@sdu.edu.cn (X.-z. Cui), 1914569734@qq.com (S.-q. Cui), 1033871383@qq.com (T. Lu), 837827723@qq.com (L. Zhang), eason_wyl@163.com (Y.-l. Wang), forzaapis@126.com (J. Li).

https://doi.org/10.1016/j.conbuildmat.2018.07.046
0950-0618/

foundation [19–21]. Some researchers have used site tests or numerical analysis to study the behaviors of geobelts-reinforced soil structures under static loads, and they confirmed the beneficial effect of reinforcement on the enhancement of bearing capacity and shear strength characteristics [22–24]. But, there is no study that has been focused on the response of soil structure reinforced with geobelts under dynamic loads.

All the studies reviewed above primarily investigated the performance of traditional geosynthetics under static and dynamic loads. Nevertheless, as geosynthetic-reinforced soil structures become more widespread globally, it becomes increasingly vital to ensure that these structures are not only safe but also offer a satisfactory level of serviceability through health monitoring. Thus, a novel concept of sensor-enabled geogrids (SEGG) has been developed based on the tensoresistivity of electrically filled polymers [25]. A self-measurement function was added to SEGG by adding a critical concentration of conductive fillers (e.g., carbon blacks and carbon nanotubes) to the polymers (e.g., polypropylene). This self-measurement function affords SEGG a unique and significant characteristic by which their tensile strain can be conveniently measured. However, an important unsolved problem remains in the referenced SEGG studies: the strain-conductivity response of SEGG materials with multiple ribs is complex, and the accuracy of self-measurement results cannot be fully ensured [26]. Therefore, to ensure the self-measurement accuracy, a new smart geosynthetic named sensor-enabled geobelts (SEGB) was developed by the authors [27]. The SEGB of high-density polyethylene (HDPE) filled with super conductive carbon black (CB) was fabricated by both industry and laboratory. In authors' previous study, a series of in-isolation tests were conducted to study its mechanical properties and tensoresistivity performance. And the pullout tests were performed using a large pullout device to investigate in-soil performance of SEGB and verify the accuracy of SEGB self-measurement.

These studies on SEGB and SEGG are solely focused on the performance under static loads. However, compared to the traditional geosynthetics, SEGB can be subjected to seismic loads during service life and more studies are needed to obtain comprehensive knowledge on SEGB. There are few evaluations on the performances of SEGB after earthquake. Though Yazdani et al. [28] studied the influence of cyclic loading on SEGG, the frequency of cyclic loading is too low to simulate seismic loads. In this paper, to simulate the seismic behavior of SEGB, a series of cyclic loading tests were performed. The factors including the prestrains, number of loading cycles and strain amplitude of cyclic load were investigated. This work aims to improve the knowledge related to the effects of earthquake on the mechanical properties and tensoresistivity performance of SEGB.

2. Materials

The materials used for SEGB included high-density polyethylene (HDPE) and the super conductive carbon black (CB). The physical properties of HDPE are shown in Table 1. Because the components of CB masterbathes and their contents are disclosed by the supplying companies, the filler content of the CB-filled SEGB in this paper was the mixing ratio of the conductive masterbatch to the HDPE instead of the actual contents. In the fabrication of SEGB, HDPE was filled with the conductive masterbatch (CB) by different weight. In factory, the masterbatch of CB was firstly mixed with HDPE until the polymer beads appeared to be evenly distributed in the mix. The mixture in the batch should be kept dry before being poured into the extruder and then be preheated and melted completely and uniformly. The temperatures in the working zones of the extruder were set to 180 °C, 185 °C, 190 °C, 200 °C, 213 °C, 205 °C, 212 °C. The compounding procedures started after reaching the target temperatures, and the pellets melted in the working zones. Once extruded, SEGB was extrusion molded.

Table 1
Physical properties of HDPE.

Density (g/cm^3)	Tensile strength (MPa)	Elongation at break (%)
0.954	26	500

Rectangle SEGB specimens (16 cm × 11 cm) with a thickness of 4 mm were molded. The specimens were wiped clean and then adhered by conductive tapes as measuring points. The surface resistance was measured with a FLUKE insulation tester. The surface resistivity is defined as follows:

$$\rho_s = R_s \frac{l}{d} \tag{1}$$

where ρ_s is the surface resistivity; R_s is the surface resistance; d is the electrode distance perpendicular to the two conductive adhesive tapes; and l is the electrode length.

Fig. 1 shows the variation curve of the surface resistivity of SEGB with the CB content [27]. It is seen that the surface resistivity of SEGB gradually decreases with the concentration of conductive fillers CB and eventually tends to stability at a critical concentration (i.e., 47.5% in Fig. 1). Based on the percolation theory [29,30], a CB conductive network which allows the electrons to be able to "flow across the polymer barrier" or "travel through a disordered network of conductive fillers" is formed at this critical concentration. At the point of 47.5%, small changes in the CB conductive network structure (e.g., due to tensile strain) can dramatically change the conductive pathways in the SEGB, which in turn can cause large changes in conductivity. Hence, in this study, the tests were performed on the SEGB with the filler concentration of 47.5%, which was the optimum CB content value.

3. Cyclic loading tests

3.1. Simulation of seismic loads

According to the previous studies [31–35], the number of significant uniform loading cycles can be considered equivalent to repetitive loads on site caused by an earthquake that has irregular stress-time history. This can be explained with the aid of Fig. 2. Fig. 2(a) shows the irregular pattern of stress with time for an earthquake. The maximum stress induced is σ_{max}. Because the effect of the irregular stress-time history shown in Fig. 2(a) is the same as the uniform stress cycles shown in Fig. 2(b), the stress-time history of earthquake can be equivalent to uniform strain–time history of cyclic stress with the maximum magnitude equal to $\beta\sigma_{max}$. Seed et al. [32] presented the relationship between the earthquake magnitude and the equivalent number and duration of loading cycles, shown in Table 2. In this study, changing the number and duration of cyclic loading simulated the five kinds of earthquake magnitudes in Table 2.

During earthquake, dynamic stress was applied on geosynthetics by the transformation of soil. Wang et al. [36] investigated the behaviors of geosynthetic-reinforced embankment during an earthquake by using centrifuge model tests. It was found that the peak strain of geosynthetics induced by earthquake was around 2%. Therefore, based on their studies, there were two strain amplitudes (i.e., 1% and 2%) used in the tests to simulate the intensity of earthquake.

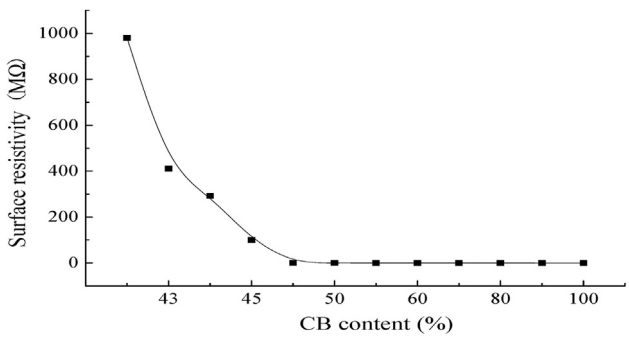

Fig. 1. Variation curve of the surface resistivity of SEGB.

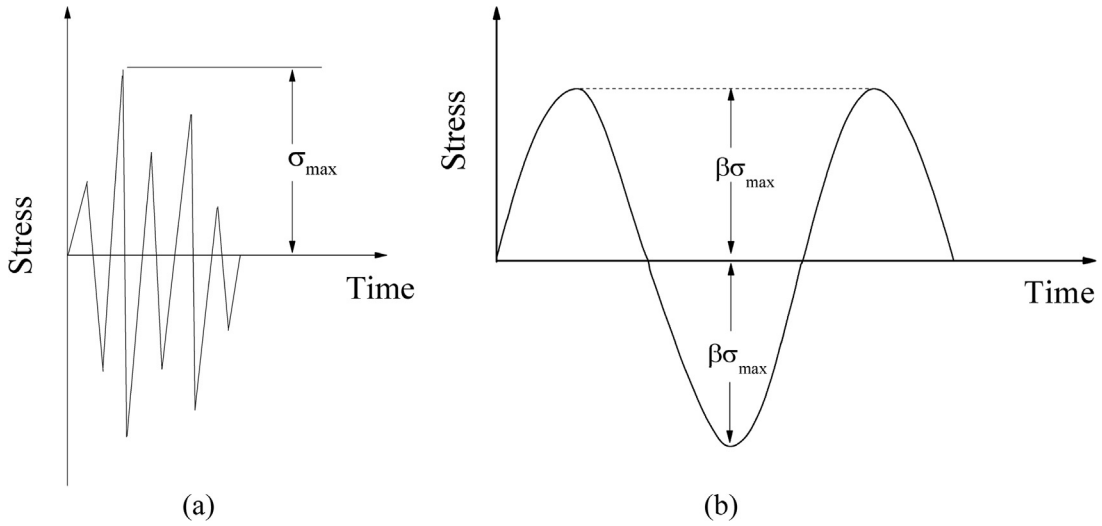

Fig. 2. Stress–time histories curves: (a) irregular stress-time history of an earthquake; (b) equivalent uniform stress–time history.

Table 2
Representative numbers of loading cycles for typical strong earthquakes.

Earthquake magnitude	Equivalent number of loading cycles	Duration (s)	Frequency (Hz)
5.5 ~ 6	5	8	0.625
6.5	8	14	0.571
7.0	12	20	0.60
7.5	20	40	0.50
8.0	30	60	0.50

Note: the number of loading cycles is divided by the duration to obtain frequency.

3.2. Prestrain

The deformation of geosynthetics induced by static loads (i.e., gravity) before earthquake can affect its post-earthquake performance. To study the influence of the initial deformation on the post-earthquake performance of SEGB, different prestrains were applied before cyclic loading tests. As the geosynthetics strain at failure of soils is typically around 2% to 6% [37,38], there are three prestrains that are designed 3%, 4% and 5%.

3.3. Testing procedure

The servo-hydraulic testing system was used for the cyclic loading test, shown in Fig. 3. The SEGB specimens used in the tests are cut from the industry-fabricated SEGB product with a blade cutter. According to the Plastics-Determination of tensile properties [39], all the SEGB specimens were limited in size to 160 mm long × 15 mm wide × 1.7 mm thick by using a blade cutter, shown in Fig. 4.

In this study, the tests included two steps: a) the monotonic stage at the constant strain rate of 1 mm/min to make the SEGB specimens reach a fixed prestrain (3%, 4% and 5%); b) cyclic loading stage using a sinusoidal function with a fixed strain amplitude (1% and 2%), for a fixed number of loading cycles N (0, 5, 8, 12, 20 and 30). Some typical whole process stress-strain curves in the tests are shown in Fig. 5.

Details of the tests in this study were summarized in Table 3. There were three kinds of prestrains (i.e. 3%, 4% and 5%) and six kinds of number of loading cycles (i.e. 0, 5, 8, 12, 20 and 30). According to Table 2, for any kind of earthquake magnitude, the relationship between equivalent number of loading cycles and frequency is determined. Therefore, the frequency varies with the number of loading cycles. In total, 33 sets of tests were performed, with each set having 3 specimens.

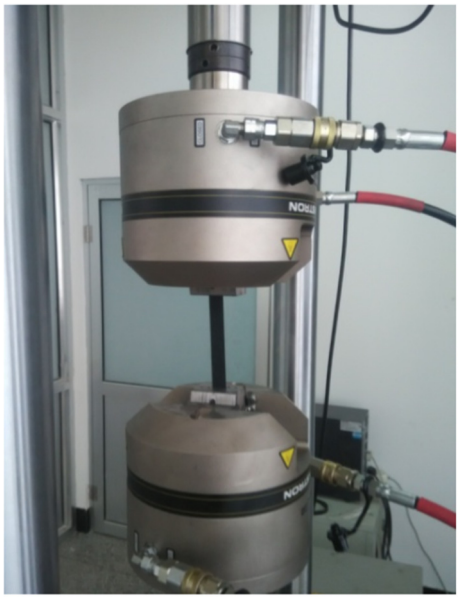

Fig. 3. Diagram of the servo-hydraulic testing system.

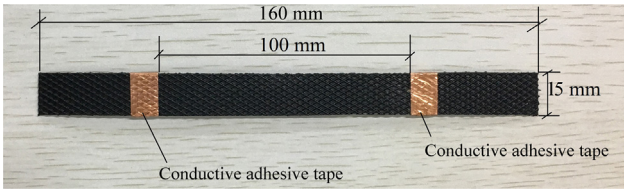

Fig. 4. SEGB specimen for cyclic loading tests.

4. Tests on the performance of SEGB

To study the mechanical and tensoresistivity performances of SEGB before and after cyclic loading, two kinds of tensile tests were conducted: (1) fast tensile tests to study the mechanical properties

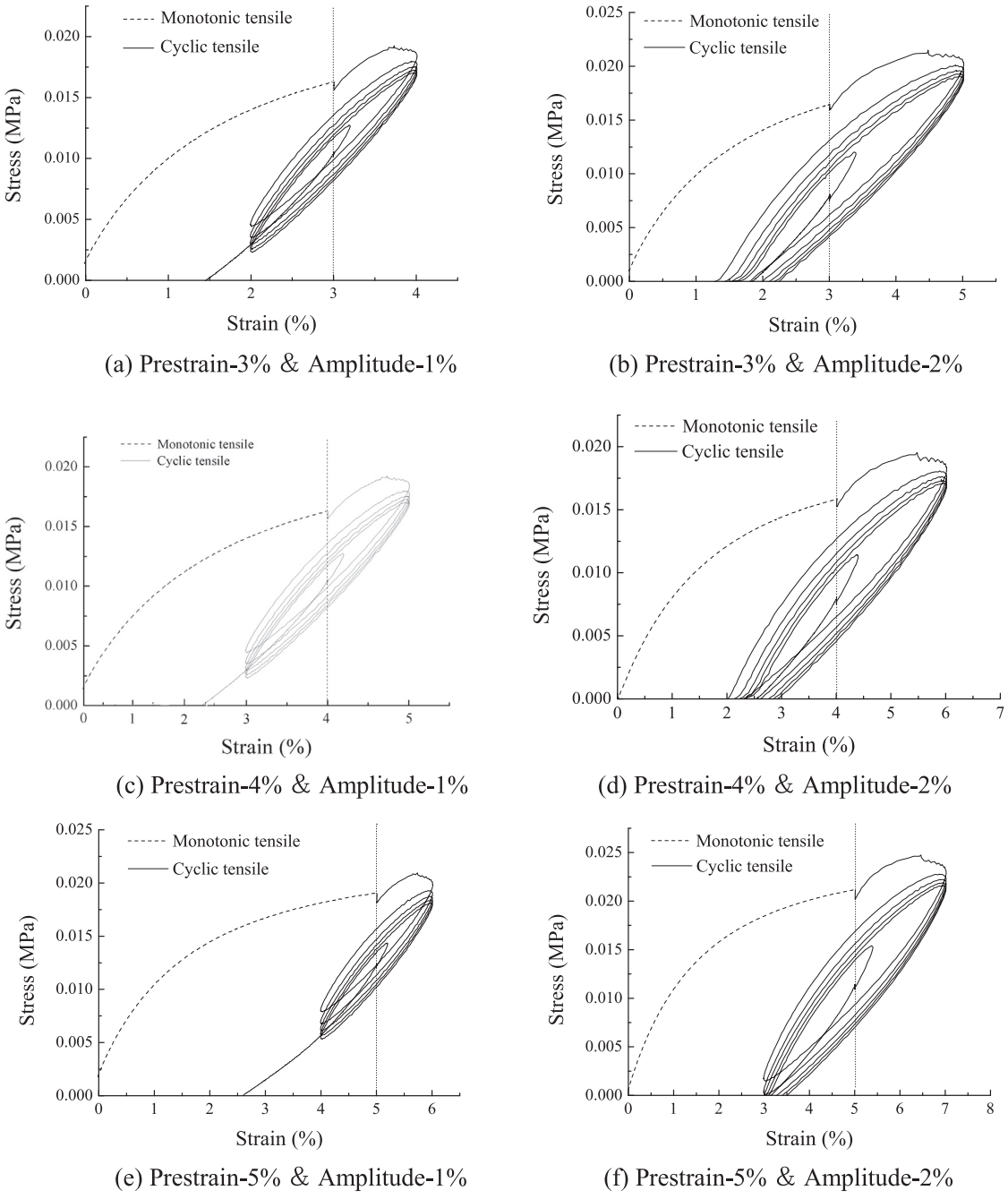

Fig. 5. Whole process stress-strain curves of SEGB.

of SEGB before and after cyclic loading, (2) slow tensile tests to study the tensoresistivity performance of SEGB before and after cyclic loading.

4.1. Fast tensile test

The tensile strength and elongation at break are the two most important performance indexes. The elongation at break indicates the ratio of the changed sample length at breakage to its original length.

To study the tensile strength and elongation at break of SEGB before and after cyclic loading, fast tensile tests were performed on a universal testing machine. According to Plastics – Determination of tensile properties [39], the tensile loading speed was 20 mm/min and was continued until the specimen broke.

4.2. Slow tensile test

The slow tensile tests were also performed on a universal testing machine and the typical load-time curve of the SEGB specimen was shown in Fig. 6. In the slow tensile test, the loading speed was cycled at 0.25 mm/min for 1 min initially and then 0.001 mm/min for 3 min, until the strain reached 10%. It can be seen that in the 0.25 mm/min loading speed phase, the tensile strain increases. In the 0.001 mm/min load phase, the strain gradually decreases. This is because in the slow loading phase, the stress relaxation gains the advantage.

The slow tensile test simulated the real load conditions with a slow loading while shortening the period as much as possible. The surface resistance was measured with a FLUKE insulation tester at the beginning of the test and the end of each loading speed cycle.

Table 3
Test cases.

Case	Earthquake magnitude	Equivalent number of loading cycles	Frequency (Hz)	Strain amplitude of cyclic load	Prestrain
1	0	0	0	0	3%
2	0	0	0	0	4%
3	0	0	0	0	5%
4	5.5–6	5	0.625	1%	3%
5	5.5–6	5	0.625	1%	4%
6	5.5–6	5	0.625	1%	5%
7	5.5–6	5	0.625	2%	3%
8	5.5–6	5	0.625	2%	4%
9	5.5–6	5	0.625	2%	5%
10	6.5	8	0.571	1%	3%
11	6.5	8	0.571	1%	4%
12	6.5	8	0.571	1%	5%
13	6.5	8	0.571	2%	3%
14	6.5	8	0.571	2%	4%
15	6.5	8	0.571	2%	5%
16	7.0	12	0.60	1%	3%
17	7.0	12	0.60	1%	4%
18	7.0	12	0.60	1%	5%
19	7.0	12	0.60	2%	3%
20	7.0	12	0.60	2%	4%
21	7.0	12	0.60	2%	5%
22	7.5	20	0.50	1%	3%
23	7.5	20	0.50	1%	4%
24	7.5	20	0.50	1%	5%
25	7.5	20	0.50	2%	3%
26	7.5	20	0.50	2%	4%
27	7.5	20	0.50	2%	5%
28	8.0	30	0.50	1%	3%
29	8.0	30	0.50	1%	4%
30	8.0	30	0.50	1%	5%
31	8.0	30	0.50	2%	3%
32	8.0	30	0.50	2%	4%
33	8.0	30	0.50	2%	5%

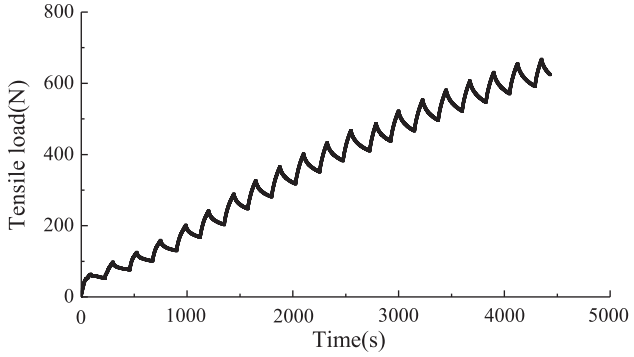

Fig. 6. Load-time curve of the SEGB specimen in the slow tensile test.

5. Results and analyses

As described above, the relationship between equivalent number of loading cycles and frequency is determined. At the same time, the variation of frequency is slight for different earthquake magnitudes. Hence, in the flowing result analyses, number of loading cycles is used to represent different earthquake magnitudes.

5.1. Mechanical properties of SEGB after cyclic loading

(1) Tensile strength

In order to compare and analyze the tensile strength of SEGB before and after cyclic loading, a ratio of tensile strength is used and defined as Eq. (2)

$$R_t = \frac{\sigma_u}{\sigma_{u0}} \tag{2}$$

where R_t is the ratio of tensile strength; σ_{u0} is the tensile strength before cyclic loading; σ_u is the tensile strength after cyclic loading.

Fig. 7 shows the variation curves of R_t with number of loading cycles. The ratio of tensile strength decreases sharply with number of loading cycles at the beginning, but then decreases slightly. It is implied that the damage of SEGB evolves quickly at the initial stage and then slowly. For the same number of loading cycles, the ratio of tensile strength of SEGB subjected to 2% amplitude is significantly less than SEGB subjected to 1% amplitude. Compared to the number of loading cycles and amplitude of cyclic loading, it is seen that prestrain has a limited influence on the reduction of tensile strength after cyclic loading.

In this study, the reduction of tensile strength after cyclic loading is less than 10%, and the maximum is 9.2% (when the prestrain is 5%, the strain amplitude of cyclic load is 2% and the number of loading cycles is 30).

(2) Elongation at break

In order to compare and analyze the elongation at break of SEGB before and after cyclic loading, a ratio of elongation at break is used and defined as Eq. (3)

$$R_e = \frac{\varepsilon}{\varepsilon_0} \tag{3}$$

where R_e is the ratio of elongation at break; ε_0 is the elongation at break before cyclic loading; ε is the elongation at the break after cyclic loading.

Fig. 8 shows the variation curves of R_e with number of loading cycles. In Fig. 8, as the number of loading cycles increases, the maximum and minimum decrement of R_e for amplitude = 1% are 1.212% and 0.514%, respectively. And with the increase of

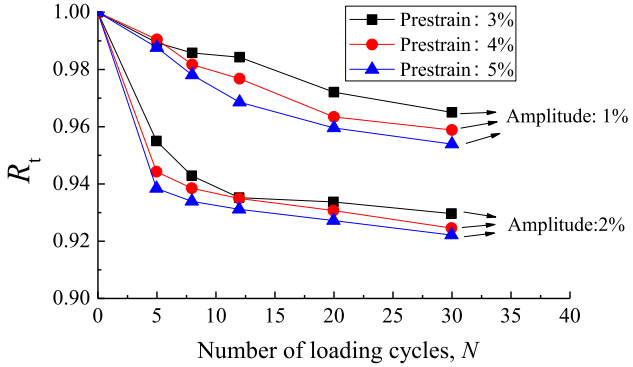

Fig. 7. Variation curves of R_t with number of loading cycles.

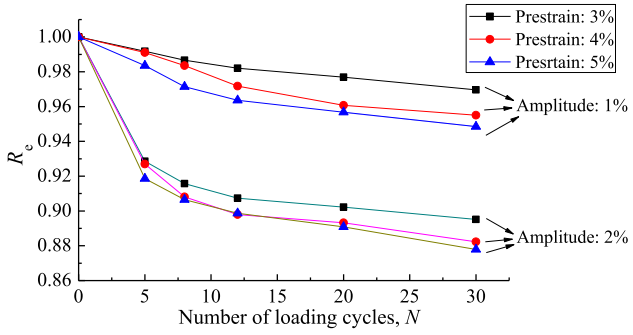

Fig. 8. Variation curves of R_e with number of loading cycles.

prestrains, the maximum and minimum decrement of R_e for amplitude = 1% are 1.45% and 0.312%, respectively. Therefore, the prestrain has the same effect on the R_e with the number of loading cycles. However, the maximum and minimum decrement of R_e for amplitude = 2%, with the increase of prestrains, are 0.645% and 0.163%, while the maximum and minimum are 1.85% and 0.612% with the number of loading cycles increasing. Hence, compared to the number of loading cycles, the prestrain has a limited impact on the R_e for amplitude = 2%. It is concluded that the prestrains contribute little to the decrements of the R_e for amplitude = 2%, while the number of loading cycles and the prestrain have same level influences on the R_e for amplitude = 1%. In

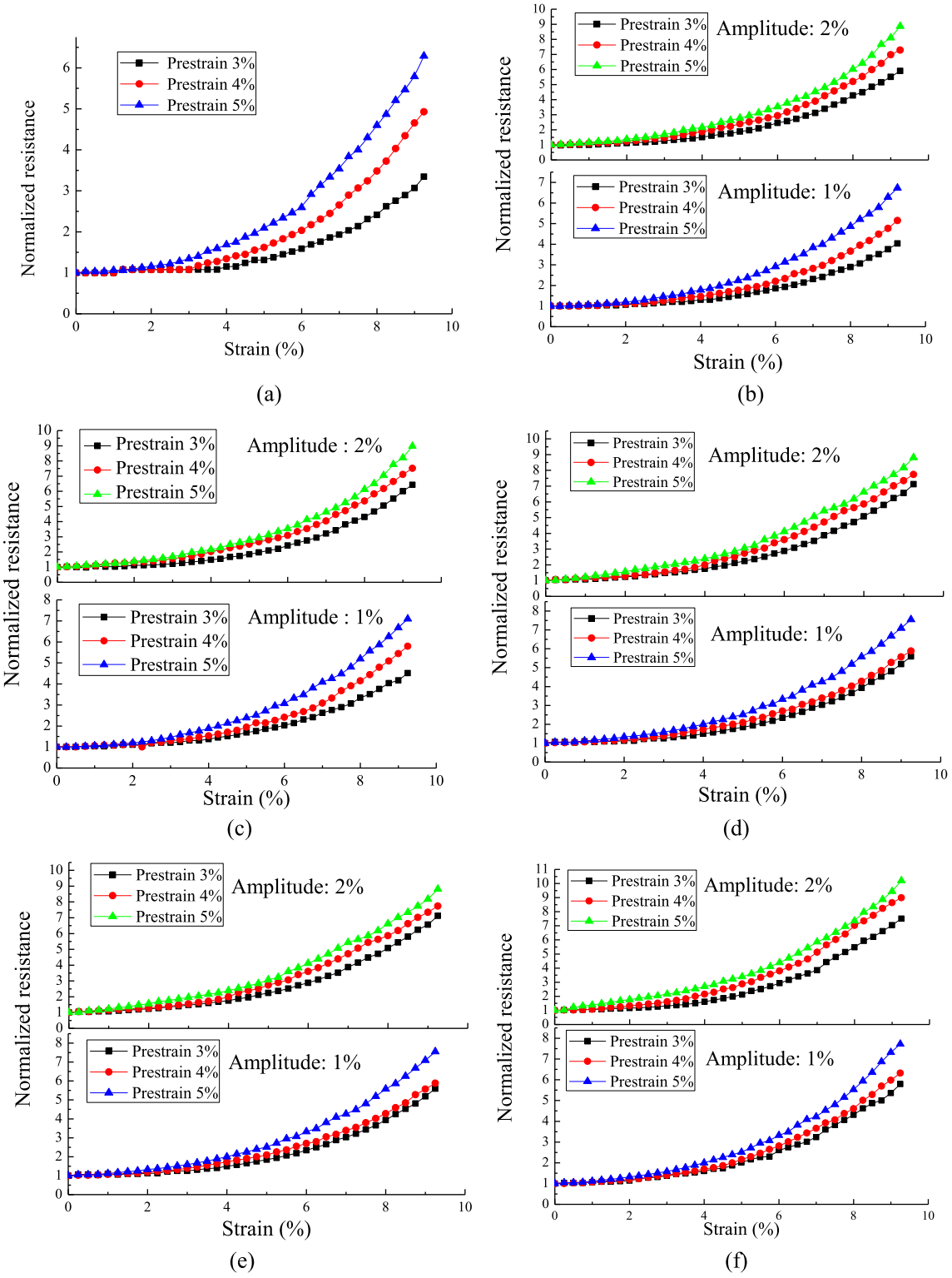

Fig. 9. Normalized resistance-strain curves of SEGB subjected to different number of loading cycles: (a) 0 cycles; (b) 5 cycles; (c) 8 cycles; (d) 12 cycles; (e) 20 cycles; (f) 30 cycles.

addition, compared to the prestrains and the number of loading cycles, the reduction of elongation at break (i.e. R_e) is significantly dependent on the amplitude of cyclic load. In this study, the reduction of the elongation at break (i.e. R_e) is 11.3% at most. The reduction of elongation at break means reduction of the ductility of SEGB after cyclic loading.

5.2. Tensoresistivity performance

In order to compare and analyze the tensoresistivity performance of SEGB, the surface resistance is normalized as Eq. (4)

$$k = \frac{R_s}{R_{s0}} \tag{4}$$

where k is the normalized resistance; R_{s0} is the original surface resistance before slow tests; R_s is the surface resistance during slow tests.

Fig. 9 shows the variation curves of normalized resistance of SEGB with strain. It can be seen that the normalized resistances slowly increase with strain at the beginning and then increases rapidly. The normalized resistance-strain curves could be fitted with a quadratic polynomial function, which is consistent with the authors' previous research [27].

It is seen from Fig. 9 that all the normalized resistance-strain curves are similar. Therefore, in this study, the normalized resistance k is divided by the normalized resistance k_{10} corresponding to the 10% strain, as shown in Fig. 10. In Fig. 10, the relationship between k/k_{10} and strain is basically unrelated to the prestrains, number of loading cycles and amplitude of cyclic load. And it can be fitted with the following quadratic polynomial function, with $r^2 = 0.96$ (r is correlation coefficient):

$$\frac{k}{k_{10}} = a\varepsilon^2 + b\varepsilon + c \tag{5}$$

where the fitting parameters $a = 0.011$, $b = 0.015$, $c = 0.135$.

In Eq. (5), k_{10} is related to the prestrain, number of loading cycles and amplitude of cyclic load. Fig. 11(a) and (b) show the variation curves of k_{10} with these variables. In Fig. 11(a), there is a sharp increase for k_{10} with number of loading cycles at the beginning and then the increasing trend becomes mild. It is implied that the damage of CB conductive networks induced by cyclic loading evolves quickly at the initial stage and then slowly. The reason is that the damage of CB conductive networks results in the increase of normalized resistances after cyclic loading [40]. For the same number of loading cycles, the normalized resistance k_{10} of SEGB subjected to 2% amplitude is significantly larger than SEGB subjected to 1% amplitude. From Fig. 11(b), it can be seen that greater

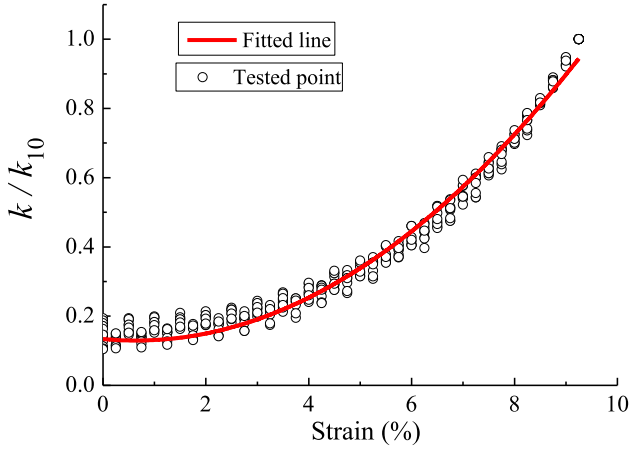

Fig. 10. Variation curves of k/k_{10} with strain for all cases.

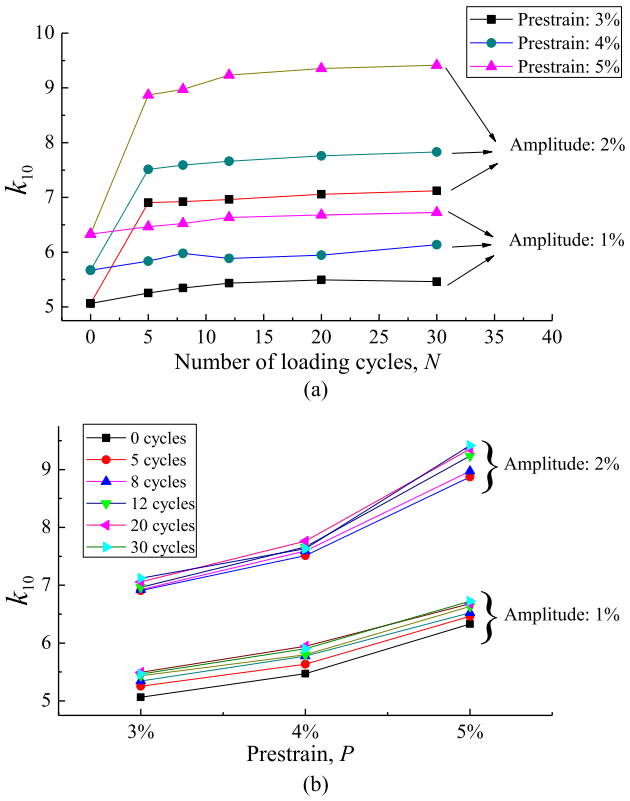

Fig. 11. Variation curves of k_{10} with: (a) number of loading cycles; (b) prestrains.

prestrains lead to the increases of normalized resistance k_{10}. In general, the electrical conductivity of SEGB becomes more sensitive to strain by increasing number of loading cycles, amplitude of cyclic load and prestrain.

It can be seen from Fig. 11 that the relationship between the normalized resistance k_{10} and number of loading cycles can be fitted with a logarithmic function, while the k_{10}-prestrain curve is well fitted with a quadratic polynomial function. Using the multiple regression analysis method, the relationship of k_{10} with the number of loading cycles, amplitude of cyclic load and prestrain was established, with $r^2 = 0.96$ (r is correlation coefficient):

$$k_{10} = 0.172 \ln N + 1.959A + 0.106P^2 + 1.82 \tag{6}$$

where N is the number of loading cycles; A is the strain amplitude of cyclic load, unit of %; P is the prestrain, unit of %.

Fig. 12 shows the relationship between the tested and fitted k_{10}. It can be seen that the fitted line agrees well with tested values.

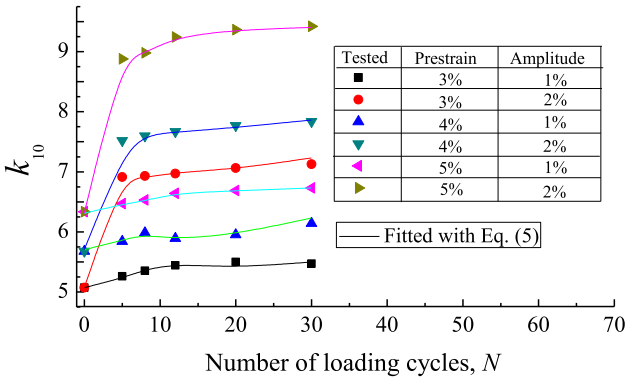

Fig. 12. Relationship between tested and fitted k_{10}.

Table 4
Verification test cases.

Case	The number of loading cycles	Frequency (Hz)	Strain amplitude of cyclic load	Prestrain
1	10	0.5	1%	1%
2	15	0.6	1%	2%
3	15	0.6	2%	2%
4	20	0.8	1%	3%
5	20	0.8	2%	3%
6	25	0.5	1%	4%
7	25	0.5	2%	4%
8	30	0.6	1%	5%
9	30	0.6	2%	5%
10	40	0.8	1%	6%
11	40	0.8	2%	6%

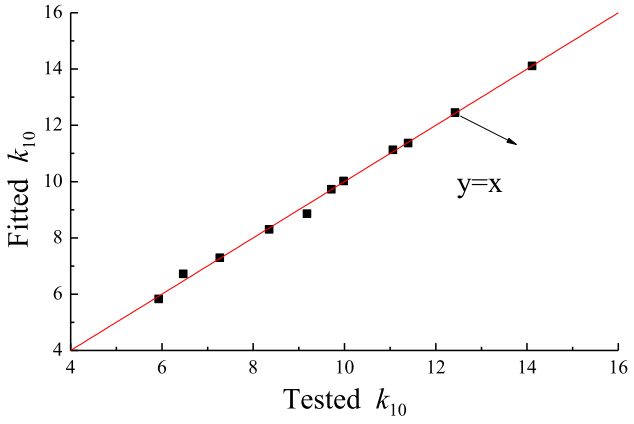

Fig. 13. Fitting effect of the uniform model.

With Eq. (5) and (6), a preliminary evaluation model of tensoresistivity performance of SEGB after cyclic loading is proposed:

$$k = \frac{R_s}{R_{s0}} = (0.172 \ln N + 1.959A + 0.106P^2 + 1.82) \times (0.011\varepsilon^2 + 0.015\varepsilon + 0.135) \quad (7)$$

To prove the correctness of Eq. (7), the verification tests have been conducted and the details were summarized in Table 4.

As a uniform model, Eq. (7) considers the influences of the prestrain, the number of loading cycles and the strain amplitude of cyclic load. Fig. 13 shows the relationship between the tested and fitted k_{10} (i.e. the normalized resistance k_{10} corresponding to the 10% strain).

Fig. 13 shows the fitting effect of Eq. (7). It can be seen that the fitted values agree well with the tested values. This model is useful for engineers to approximately estimate the tensoresistivity performance of SEGB after cyclic loading.

6. Conclusions

In this study, a series of cyclic loading tests were performed to study the influence of cyclic loading on the performances of SEGB. Based on the test results, a preliminary model was proposed to evaluate the tensoresistivity performance of SEGB after cyclic loading. The following conclusions were drawn as follows:

(1) Compared to the SEGB before cyclic loading, both the tensile strength and elongation at break of the SEGB after cyclic loading decreased with number of loading cycles and amplitude of cyclic load. However, prestrains have a limited influence on the mechanical properties of SEGB.

(2) After cyclic loading, the electrical conductivity of SEGB becomes more sensitive to strain by increasing the number of loading cycles, amplitude of cyclic load and prestrains. The relationship of the normalized resistance with the number of loading cycles and prestrain can be fitted with a logarithmic function and a quadratic polynomial function, respectively.

Conflict of interest

The authors declared that they have no conflicts of interest to this work.

We declare that we do not have any commercial or associative interest that represents a conflict of interest in connection with the work submitted.

Acknowledgments

This work is supported by the Natural Science Foundations of China (Nos. 51778346, 51479105, 51279094), the key research and development program of Shandong Province (2017GGX50102), the Fund of the Science, Technology and Innovation Commission of ShenZhen Municipality (JCYJ20160429183630760) and the Science Fund for Distinguished Young Scholars of Shandong Province (No. JQ201416).

References

[1] J.N. Mandal, K.S. Jambale, Analysis of a geosynthetic reinforced soil wall by the limit equilibrium method, Constr. Build. Mater. 6 (1992) 173–177.
[2] G.R. Carter, J.H. Dixon, Oriented polymer grid reinforcement, Constr. Build. Mater. 9 (1995) 389–401.
[3] A. Hegde, Geocell reinforced foundation beds-past findings, present trends and future prospects: a state-of-the-art review, Constr. Build. Mater. 154 (2017) 658–674.
[4] L. Zhang, M. Zhao, C. Shi, H. Zhao, Bearing capacity of geocell reinforcement in embankment engineering, Geotext. Geomembr. 28 (2010) 475–482.
[5] J.W. Cowland, S.C.K. Wong, Performance of a road embankment on soft clay supported on a geocell mattress foundation, Geotext. Geomembr. 12 (1993) 687–705.
[6] H.I. Ling, Z. Liu, Performance of geosynthetic-reinforced asphalt pavements, J. Geotech. Geoenviron. Eng. 127 (2001) 177–184.
[7] M. Adams, Performance of a prestrained geosynthetic reinforced soil bridge pier, in: Mechanically Stabilized Backfill, Balkema, Rotterdam, Netherlands, 1997, pp. 35–53.
[8] P.J.P. Gotteland, P. Gourc, Villard Geosynthetic reinforced structures as bridge abutments: full scale experimentation and comparison with modelisations, in: Mechanically Stabilized Backfill, Balkema, Rotterdam, Netherlands, 1997, pp. 25–34.
[9] K. Ketchart, J.T.H. Wu, Performance of geosynthetics reinforced soil bridge pier and abutment, Denver, Colorado, USA, in: Mechanically Stabilized Backfill, Balkema, Rotterdam, Netherlands, 1997, pp. 101–116.
[10] M. Adams, J. Nicks, T. Stabile, J. Wu, W. Schlatter, J. Hartmann, Geosynthetic Reinforced Soil Integrated Bridge System Interim Implementation Guide, U.S. Dept. of Transportation, Washington, DC, 2011. FHWA-HRT-11-026.
[11] J.E. Nicks, M.T. Adams, P.S.K. Ooi, T. Stabile, Geosynthetic Reinforced Soil Performance Testing – Axial Load Deformation Relationships, U.S. Dept. of Transportation, Washington, DC, 2013. FHWA-HRT-13-066.
[12] H. Liu, Analyzing the reinforcement loads of geosynthetic-reinforced soil walls subject to seismic loading during the service life, J. Perform. Constr. Facil. ASCE 23 (2009) 292–302.
[13] M. Sabermahani, A. Ghalandarzadeh, A. Fakher, Experimental study on seismic deformation modes of reinforced-soil walls, Geotext. Geomembr. 27 (2009) 121–136.
[14] C.C. Huang, J. Horng, W. Chang, J. Chiou, C. Chen, Dynamic behavior of reinforced walls e horizontal displacement response, Geotext. Geomembr. 29 (2011) 257–267.
[15] E. Guler, O. Selek, Reduced-scale shaking table tests on geosynthetic reinforced soil walls with modular facing, J. Geotech. Geoenviron. Eng. 140 (2014) 1–11.
[16] G.M. Latha, P. Santhanakumar, Seismic response of reduced-scale modular block and rigid faced reinforced walls through shaking table tests, Geotext. Geomembr. 43 (2015) 307–316.
[17] A.K. Panah, M. Yazdi, A. Ghalandarzadeh, Shaking table tests on soil retaining walls reinforced by polymeric strips, Geotext. Geomembr. 43 (2015) 148–161.
[18] L. Wang, G. Chen, S. Chen, Experimental study on seismic response of geogrid reinforced rigid retaining walls with saturated backfill sand, Geotext. Geomembr. 43 (2015) 35–45.

[19] X.Z. Huang, F.X. Yan, J.Z. Fan, Applying research of geobelt-reinforced gravel cushion in soft foundation, in: Proceeding of Chinese-Japan Geotechnical Engineering International Conference, Tongji University Press, Shanghai, 2005, pp. 358–361.
[20] X.Z. Huang, J. Han, F.X. Yan, et al., Stability analysis of geobelt-reinforced cushion foundation, in: Ground Improvement and Geosynthetics, ASCE, Geotechnical Special Publication, Shanghai, 2010, pp. 287–294. 207.
[21] Z.G. Jin, Construction technology of reinforced foundation treatment, Shanxi Arch. 29 (2) (2003) 38–39.
[22] X.H. Bai, X.Z. Huang, W. Zhang, Bearing capacity of square footing supported by a geobelt-reinforced crushed stone cushion on soft soil, Geotext. Geomembr. 38 (3) (2013) 37–42.
[23] X.Z. Huang, X.H. Bai, Study of shear strength characteristics of geobelt reinforced crushed gravel soil, Rock Soil Mech. 26 (9) (2005) 1464–1468.
[24] T.W. Zhang, Research on sandstone cushion by reinforced with geotechnical band and finite element analysis, Constr. Technol. 43 (7) (2014) 83–86.
[25] K. Hatami, B.P. Grady, M.C. Ulmer, Sensor-enabled geosynthetics: use of conducting carbon networks as geosynthetic sensors, J. Geotech. Geoenviron. Eng. 135 (2009) 863–874.
[26] Q. Chen, Discussion of "Sensor-enabled geosynthetics: use of conducting carbon networks as geosynthetic sensors" by Kianoosh Hatami, Brian P. Grady, and Matthew C. Ulmer, J. Geotech. Geoenviron. Eng. 137 (2011) 435–436.
[27] X.Z. Cui, S.Q. Cui, Q. Jin, Y.L. Wang, L. Zhang, Z.X. Wang, Laboratory tests on the engineering properties of sensor-enabled geobelts (SEGB), Geotext. Geomembr. 46 (2018) 66–76.
[28] H. Yazdani, K. Hatami, E. Khosravi, K. Harper, B.P. Grady, Strain-sensitive conductivity of carbon black-filled PVC composites subjected to cyclic loading, Carbon 79 (2014) 393–405.
[29] J.C. Huang, Carbon black filled conducting polymers and polymer blends, Adv. Polym. Technol. 21 (2002) 299–313.
[30] H. Yazdani, K. Hatami, B.P. Grady, Sensor-enabled geogrids for performance monitoring of reinforced soil structures, J. Test. Eval. 44 (2016) 391–401.
[31] K.L. Lee, K. Chan, Number of equivalent significant cycles in strong motion earthquakes, in: Proceedings, International Conference on Microzonation, Seattle, Washington, 1972, pp. 609–627.
[32] H.B. Seed, I.M. Idriss, F. Makdisi, N. Banerjee, Representation of Irregular Stress – Time Histories by Equivalent Uniform Stress Series in Liquefaction Analysis, Earthquake Engineering Research Center, University of California, Berkeley, 1975. Report No. EERC 75–29.
[33] H.B. Seed, Evaluation of Soil Liquefaction Effects on Level Ground During Earthquakes, ASCE National Convention, 1976, pp. 1–104. Preprint No. 2752.
[34] H.B. Seed, Soil liquefaction and cyclic mobility evaluation for level ground during earthquakes, J. Geotech. Eng. Div., ASCE 105 (1979) 102–155.
[35] J.E. Valera, N.C. Donovan, Soil liquefaction procedures – a review, J. Geotech. Eng. Div., ASCE 103 (1977) 607–625.
[36] L.P. Wang, G. Zhang, J.M. Zhang, Centrifuge model tests of geotextile-reinforced soil embankments during an earthquake, Geotext. Geomembr. 29 (2011) 222–232.
[37] K. Hatami, R.J. Bathurst, Development and verification of a numerical model for the analysis of geosynthetic-reinforced soil segmental walls under working stress conditions, Can. Geotech. J. 42 (4) (2005) 1066–1085.
[38] D. Wanatowski, J. Chu, Stress-strain behavior of a granular fill measured by a new plane-strain apparatus, Geotech. Test. J. 29 (2) (2006) 149–157.
[39] AQSIQ (General Administration of Quality Supervision, Inspection and Quarantine of the People's Republic of China) & SAC (Standardization Administration of the People's Republic of China) (2006). GB/T 1040.1-2006: Plastics – Determination of tensile properties. Standards Press of China, Beijing (in Chinese).
[40] V. Jha, A.G. Thomas, M. Bennett, J.J.C. Busfield, Reversible electrical behavior with strain for a carbon black–filled rubber, J Appl Polym Sci 116 (2010) 541–546.